Constraining the Inert Doublet Model using Vector Boson Fusion

Daniel Dercks and Tania Robens

(Dated: December 24, 2019)

In this work, we use a recast of the Run II search for invisible Higgs decays within Vector Boson Fusion to constrain the parameter space of the Inert Doublet model, a two Higgs doublet model with a dark matter candidate. When including all known theoretical as well as collider constraints, we find that the above can rule out a relatively large part in the m_H, λ_{345} parameter space, for dark scalar masses $m_H \leq 100\,\mathrm{GeV}$. Including the latest dark matter constraints, a smaller part of parameter space remains which is solely excluded from the above analysis. We also discuss the sensitivity of monojet searches and multilepton final states from Run II.

I.   INTRODUCTION

The Inert Doublet model (IDM) is one of the most straighforward extensions of the Standard Model (SM) [1–3]. It belongs to the class of Two Higgs Doublet Models (2HDM) which contain two $SU(2)$ doublets in the scalar sector. One of these doublets, ϕ_S, has a nonvanishing vacuum expectation value (vev) which is responsible for the spontaneous breaking of electroweak symmetry in the Standard Model while the second scalar doublet ϕ_D by construction does not acquire such a vev. This second doublet is hence not involved in the spontaneous mass generation in the Standard Model and does not couple to the SM fermions.

Within this model we impose an additional Z_2 symmetry, labelled D-symmetry, defined via the transformation

$$\phi_D \to -\phi_D, \ \phi_S \to \phi_S, \ \text{SM} \to \text{SM}, \tag{1}$$

which should be respected by the Lagrangian and the vacuum.

As electroweak symmetry breaking in this model proceeds completely analogous to the SM without the second doublet, ϕ_S provides the SM-like Higgs particle and is assumed to be even under the D symmetry. The second *inert* or *dark doublet* contains two charged and two neutral scalars and as they are odd under the imposed D-parity, its lightest neutral component provides a natural candidate for dark matter (DM). It provides a "perfect example" of a WIMP [4–7], and leads to an interesting pattern for the evolution of the Universe, towards the Inert phase as given by the IDM, with one, two or three phase transitions [8]. Furthermore, the IDM can provide a strong first-order phase transition [9–13] as required by the Sakharov conditions to generate a baryon asymmetry of the Universe. After the discovery of a SM-like Higgs particle in 2012, many studies have been performed in the context of the IDM which use Higgs measurements as well as astrophysical observations, see e.g. [14–23].[1] In addition, proposals were made how to search for dark scalars at the LHC in leptonic final states [15, 22, 28–31] and in single or dijet channels [32, 33].

Recently, also the important issue of vacuum (meta-) stability in the IDM has been discussed, and it was found that additional, possibly heavy scalars can have a strong impact on it [19, 34–36].[2]

While the model is intruiging per se and in spite of benchmark scenarios for the current LHC run [22, 39], it has not yet been studied explicitly by the LHC collaborations. However, recasts of other BSM searches with similar topologies have been presented in the literature, with prominent examples for searches for supersymmetric particles at LEP [40] as well as the first LHC run [20].

In this work, we present a recast of the Run II analyses presented in Ref. [41] by the CMS collaboration which target an invisibly decaying SM-like Higgs boson produced in vector boson fusion (VBF), and Ref. [42] by the ATLAS collaboration which focusses on monojet final states. We reinterpret the results of these searches within the IDM by making use of the `CheckMATE` [43, 44] framework.

The regions considered in this work are tested against all currently available theoretical and experimental constraints, with scan procedure and limits as described in Refs. [22, 23, 45].

We explore the reach of the above searches for the model's parameter space and identify regions which cannot be excluded by any of the other tested constraints. Finally, we briefly comment on other experimental BSM searches at LHC Run II that could be used as recasts for the IDM and are expected to yield further constraints on its parameter space.

---

[1] Recent analyses for models which extend the IDM by an additional singlet have been performed in [24–27].
[2] Similar solutions can be found in a simple singlet extension of the SM Higgs sector, cf. e.g. [37, 38] and references therein.

II.   THE MODEL

Imposing symmetry under the D-transformation given in Eq. (1), the full scalar potential of the IDM is given by

$$
\begin{aligned}
V(\phi_S, \phi_D) = & \\
& -\frac{1}{2}\left[m_{11}^2(\phi_S^\dagger\phi_S) + m_{22}^2(\phi_D^\dagger\phi_D)\right] + \frac{\lambda_1}{2}(\phi_S^\dagger\phi_S)^2 \\
& +\frac{\lambda_2}{2}(\phi_D^\dagger\phi_D)^2 + \lambda_3(\phi_S^\dagger\phi_S)(\phi_D^\dagger\phi_D) + \lambda_4(\phi_S^\dagger\phi_D)(\phi_D^\dagger\phi_S) \\
& +\frac{\lambda_5}{2}\left[(\phi_S^\dagger\phi_D)^2 + (\phi_D^\dagger\phi_S)^2\right].
\end{aligned}
\tag{2}
$$

In this formulation, all parameters are real (see e.g. [8]).

Depending on the signs and values of the individual parameters in $V(\phi_S, \phi_D)$, the minimisation conditions may result in different vacuum configurations where none, one or both vevs of ϕ_S or ϕ_D are non-vanishing. Within this work, we focus on the IDM realisation $\langle\phi_S\rangle \neq 0, \langle\phi_D\rangle = 0$, for which the decomposition around the vacuum state is given by

$$
\phi_S = \begin{pmatrix} \phi^+ \\ \frac{1}{\sqrt{2}}(v + h + i\xi) \end{pmatrix}, \phi_D = \begin{pmatrix} H^+ \\ \frac{1}{\sqrt{2}}(H + iA) \end{pmatrix}.
\tag{3}
$$

Here, $v = 246\,\mathrm{GeV}$ denotes the SM vacuum expectation value and the scalar field component of ϕ_S contains the SM-like Higgs boson h with mass

$$
m_h^2 = \lambda_1 v^2 = m_{11}^2,
\tag{4}
$$

fixed by the experimentally observabed value of $125.1\,\mathrm{GeV}$.

In addition to the components known from the Standard Model, the second scalar doublet of the IDM, ϕ_D, contains four *dark* or *inert* scalar field components $H, A, H^\pm$ with masses given as follows:

$$
m_{H^\pm}^2 = \frac{1}{2}\left(\lambda_3 v^2 - m_{22}^2\right),
\tag{5}
$$

$$
m_A^2 = m_{H^\pm}^2 + \frac{1}{2}\left(\lambda_4 - \lambda_5\right)v^2 = \frac{1}{2}(\bar{\lambda}_{345}v^2 - m_{22}^2),
\tag{6}
$$

$$
m_H^2 = m_{H^\pm}^2 + \frac{1}{2}\left(\lambda_4 + \lambda_5\right)v^2 = \frac{1}{2}(\lambda_{345}v^2 - m_{22}^2),
\tag{7}
$$

where we have defined

$$
\lambda_{345} := \lambda_3 + \lambda_4 + \lambda_5; \bar{\lambda}_{345} := \lambda_3 + \lambda_4 - \lambda_5.
$$

While their interactions with the Standard Model vector bosons can be derived from the gauge kinetic term in the Lagrangian, the absence of any gauge invariant Yukawa-like interaction between ϕ_D and the Standard Model fermion sector prohibits any tree level interactions between these four dark particles and the SM fermions. Moreover, due to the exact D-symmetry the lightest neutral scalar cannot decay and may therefore provide a candidate for dark matter.[3] Note that, contrarily to generic Two-Higgs-Doublet-Models which denote H/A as the scalar/pseudoscalar components of a doublet, we cannot make such a unique idenfication here as there is no interaction of ϕ_D with the Standard Model fermions. In fact, we can swap the roles of H and A by making the replacement $\lambda_5 \leftrightarrow -\lambda_5$, cf. Appendix A.

---

[3] Charged DM has been strongly limited by astrophysical analyses [46].

Within this work, we make the choice $m_H < m_A, m_{H^\pm}$ and assume H to be the DM candidate. According to Eqs. (5-7), this choice implies the relations $\lambda_5 < 0$ and $\lambda_{45} := \lambda_4 + \lambda_5 < 0$. The parameters λ_{345} and $\bar{\lambda}_{345}$ are related to the triple and quartic coupling between the SM-like Higgs h and the DM candidate H or the scalar A, respectively. λ_3 is relevant for the h interaction with the charged scalars $H^\pm$. Lastly, the parameter λ_2 describes the quartic self-couplings of dark particles. A list of all relevant Feynman rules for this model is provided in Appendix A.

Starting from the general scalar potential in Eq. (2), the IDM has 7 degrees of freedom. As ϕ_S plays the same role as the SM Higgs doublet for electroweak symmetry breaking, the two parameters m_h and v are fixed by the Higgs mass measurement and electroweak precision data, respectively. We are therefore left with 5 degrees of freedom which we choose to be the physical parameters

$$(m_H, m_A, m_{H^\pm}, \lambda_2, \lambda_{345}).$$

From these the corresponding dependent values of the other theory parameters can be derived by applying the relations given above.

III.   CONSTRAINTS

As has been widely discussed in the literature, the IDM is subject to numerous constraints which can be derived from both theoretical grounds as well as experimental results. We briefly remind the reader of these constraints here and refer to the literature [2, 4–6, 15, 21–23, 28, 30–33, 45, 47–67] for further details.

The constraints we use in this work have been extensively discussed in Refs. [22, 23, 45] and we refer the reader to these references for more detailed explanations. Here, we only summarise all relevant constraints and point to updates on experimental limits whenever applicable. The calculation of the IDM spectrum and tests of several of the below bounds have been obtained using 2HDMC [68].

A.   Theoretical constraints

We apply the following theoretical constraints:

- The vacuum of the model needs to be bounded from below.[4] These lead to the conditions

$$\lambda_1 > 0, \lambda_2 > 0, \lambda_3 + \sqrt{\lambda_1 \lambda_2} > 0, \lambda_{345} + \sqrt{\lambda_1 \lambda_2} > 0 \tag{8}$$

- All couplings must allow for a perturbative discussion which is why we restrict all couplings to be smaller than 4π.

- All $2 \rightarrow 2$ scalar scattering processes must not violate perturbative unitarity and we apply standard bounds as implemented in 2HDMC.

- In generic Two Higgs Doublet Models, several vacua can coexist. The tree level condition to be in the inert vacuum has been calculated in

  [8, 55, 56]

$$\frac{m_{11}^2}{\sqrt{\lambda_1}} \geq \frac{m_{22}^2}{\sqrt{\lambda_2}} \tag{9}$$

---

[4] The conditions are applied at tree level; see e.g. Refs. [19, 35] for a discussion of changes using higher-order predictions.

Here, m_{11} and m_{22} can directly be derived from Eqs. (4) - (7) and the above condition translates to

$$\lambda_{345} \leq \frac{\sqrt{\lambda_2}\, m_h\, v + 2m_H^2}{v^2}$$

The above constraint links the value of λ_{345} and the dark scalar mass to the coupling λ_2 which describes self-couplings in the scalar sector and has no influence on collider phenomenology (see e.g. the discussion in [45]). Requiring the Higgs self-coupling vertices to acquire maximally allowed values of 4π leads e.g. to $\lambda_2 \lesssim 4$ [22]. This bound, in the parameter region with relatively light dark scalars with masses $m_H \lesssim 100\,\text{GeV}$, would result in $\lambda_{345} \leq \mathcal{O}(1)$. Note, however, that this bound is not completely mandatory. Several minima may coexist (see e.g. [69, 70]) and the inert one may only be a local one as long as the transition time to the global non-inert minimum is sufficiently large. Moreover, the above condition may be significantly altered at next-to-leading order, see e.g. Refs. [60, 71]. The next-to-leading order effects are however quite involved and can not easily be generalized, but need to be recalculated on a case-by-case basis [5]. In this work, we focus on current constraints from LHC searches that are independent of λ_2; we therefore also consider values of $\lambda_{345} \gtrsim 1$. In case of a discovery, a detailed analysis would be needed in order to correctly evaluate the above condition beyond leading order, see e.g. related studies in Refs. [71, 72].

B.   Experimental constraints

In addition to the theoretical bounds listed above, several experimental observations put tight constraints on the parameter space of the IDM:

- We fix the mass of the SM-like Higgs boson h to

$$m_h = 125.1\,\text{GeV} \tag{10}$$

  in agreement with the results from the LHC experiments [73]. Note that this has already been accounted for when we chose $(m_H, m_A, m_{H^\pm}, \lambda_2, \lambda_{345})$ as the five degrees of freedom of the IDM.

- We furthermore require the total width of the 125 GeV Higgs to obey Ref. [74]

$$\Gamma_{\text{tot}} \leq 9\,\text{MeV}$$

  which is applicable in those regions of parameter space which predict additional decays of the SM-like Higgs boson.

- Furthermore, we take into account strong bounds from the measured total widths of the electroweak SM gauge bosons, cf. e.g. Ref. [75], by forbidding potentially dangerous kinematic mass configurations via the following hard constraints:

$$m_{A,H} + m_{H^\pm} \geq m_W, \tag{11}$$
$$m_A + m_H \geq m_Z, \tag{12}$$
$$2m_{H^\pm} \geq m_Z. \tag{13}$$

- We furthermore require a $2\,\sigma$, i.e. 95% C.L., agreement with electroweak precision observables, parameterized through the electroweak oblique parameters S, T and U [76–79].

---

[5] We thank P. Ferreira and B. Swiezewska for useful discussions regarding this point.

- In order to evade bounds from long-lived charged particle searches, we conservatively set an upper limit on the charged scalar lifetime of $\tau \leq 10^{-12}\, s$, to guarantee decay before the innermost detector layer. This translates to a lower bound on the total decay width of the charged scalar $H^{\pm}$ of $\Gamma_{\text{tot}} \geq 6.58 \times 10^{-13}\, \text{GeV}$. Mass dependent bounds on the charged scalar lifetime have been studied in detail in Ref. [67].

- A bound on the lower mass of $m_{H^{\pm}}$ has been derived in Ref. [80]. Although a more dedicated analysis of this bound within the current models' framework would be required, we take $m_{H^{\pm}} \geq 70\, \text{GeV}$ as a conservative lower limit.

- We also require agreement with the null-searches from the LEP, Tevatron, and LHC experiments using `HiggsBounds-5.2.0beta` [81–84], including all experimental bounds up to Moriond 2017.[6]

- We update the limits on the invisible decay of m_h and take the results presented in Ref. [86] which require $\text{BR}_{h \to \text{inv}} \leq 0.24$.

- Furthermore, we apply new limits on the branching ratio $h \to \gamma\gamma$ taken from [87] and require $\mu = 1.14^{+0.19}_{-0.18}$. Since within the IDM the production cross sections of the SM-like Higgs are unaffected, we use the bound on μ in combination with the Standard Model value [39] of $\text{BR}\,(h \to \gamma\gamma) = 2.270 \times 10^{-3}$ and require

$$\text{BR}\,(h \to \gamma\gamma) \in [1.77; 3.45] \times 10^{-3} \tag{14}$$

  at the two-sigma level.

- In addition, we require agreement within $2\,\sigma$ for the 125 GeV Higgs signal strength measurements. For this, we make use of the publicly available tool `HiggsSignals-2.2.1beta` [88], and require $\Delta\chi^2 \leq 11.3139$, corresponding to the 95% confidence level of a 5-dimensional fit.[7]

- We also include limits on the model's parameter space that have been obtained in previous reinterpretations of collider dark matter searches, predominantly within supersymmetric scenarios. Major limits stem from the reinterpretation of a LEP analysis [40] within the IDM framework [52]. This particularly rules out all regions where

$$m_A \leq 100\,\text{GeV}, \tag{15}$$
$$m_H \leq 80\,\text{GeV}, \tag{16}$$
$$\Delta m(A, H) \geq 8\,\text{GeV} \tag{17}$$

  are simultaneously fulfilled.

- After taking into account all the above limits we are outside of the region excluded due to the recent reinterpretation of the SUSY analysis from LHC Run I [20].

- We apply dark matter relic density limits obtained by the Planck experiment [89]:

$$\Omega_c\, h^2 = 0.1200 \pm 0.0012 \tag{18}$$

  In this work, we do not require the dark matter candidate of the IDM to provide the full relic density, but use it as an upper limit[8]. Being conservative, we require

$$\Omega_c\, h^2 \leq 0.1224, \tag{19}$$

---

[6] Please see the tool's documentation material in Ref. [85] for a detailed discussion of the included limits.

[7] We used a combination of Run I combination, Run II, and simplified template cross sections within `HiggsSignals`.

[8] In such a scenario, additional dark matter candidates would be needed in order to account for the missing relic density; cf. e.g. Ref. [90] for a dedicated discussion of such scenarios within a supersymmetric setup.

which corresponds to not overclosing the universe at 95 % confidence level. In addition to this bound, we specifically identify those regions which reproduce the observed DM density within the 2 σ interval around the above best fit value value. The dark matter relic density has been calculated using `MicrOmegas` version 4.3.5 [91].

- Regarding direct detection dark matter constraints, we compare to the most recent results of XENON1T [92].[9]

  As before, we consider the possibility of a multi- component dark matter scenario in which the IDM only makes up for a fraction of the total dark matter relic density. In this case, the upper limit from direct detection depends on the actual DM relic density for the specific point in parameter space; therefore, we have to introduce a rescaling factor, leading to the (relic density dependent) limit

$$\sigma\left(m_H, \{\ldots\}\right) \leq \sigma^{\mathrm{XENON1T}}(m_H) \times \frac{\Omega^{\mathrm{Planck}}}{\Omega(m_H, \{\ldots\})}, \tag{20}$$

  where m_H now denotes the dependence on the mass of our dark matter candidate H and $\{\ldots\}$ is short for all other parameters specifying the respective IDM parameter point.[10] Direct detection cross sections are again obtained using `MicrOmegas`.

The scan setup has been described in great detail in Ref. [22]. To determine allowed regions in parameter space, we follow the procedure discussed therein, including the experimental updates listed above.

IV.   LHC ANALYSIS OF VBF AND MONOJETS

In this work, we choose to constrain ourselves to cases for dark matter candidate masses $m_H \leq 100\,\mathrm{GeV}$. Due to the relatively high production cross section in such cases, these will be the regions which are most sensitive to collider searches (see e.g. [30, 32, 33, 98] for recent work on low mass scenario studies at the LHC).

We here concentrate on the 13 TeV CMS search for an invisibly decaying Higgs [41] produced through vector boson fusion (VBF) and a 13 TeV ATLAS search [42] for dark matter candidates in the monojet channel. These respectively lead to the collider signatures

$$p\,p \rightarrow j\,j\, + \not{E}_T, \quad \text{(VBF)} \tag{21}$$

$$p\,p \rightarrow j\, + \not{E}_T, \quad \text{(Monojet)}. \tag{22}$$

In this study, we mainly focus on the VBF channel which, as we show later, provides the strongest sensitivity. We however also determine bounds on the IDM using a monojet reinterpretation for comparision. A dedicated exploration of this channel including sensitivity prospects of the high luminosity LHC can be found in Ref. [32].

A.   Features of the VBF Channel

The two jets in the VBF channel typically have a large separation in pseudorapidity. The corresponding cuts used in the above analysis are listed in table I. These form a "Cut-and-Count analysis" and a "Shape analysis". The former is designed for a large signal-to-background ratio and requires a large value for the invariant mass m_{jj} of the jet pair, whilst the latter defines several signal regions binned in m_{jj} and used collectively in a fit. Using these signatures, the CMS collaboration finds an upper limit on the invisible Higgs branching ratio of $\mathrm{BR}^{\mathrm{max}}_{h \to \mathrm{inv}} = 0.53$ using the

---

[9] We here use the data available from Ref. [93] in a digitalized format. In our code, we use an approximation function which reproduces these constraints on the per-cent level.

[10] See also Refs. [90, 94–97].

Requirement	Cut-and-Count	Shape
Leading Jet p_{T}	>80 GeV	
Second Jet p_{T}	>40 GeV	
$E_{\mathrm{T}}^{\mathrm{miss}}$	>250 GeV	
$|\Delta\phi_{j,E_{\mathrm{T}}^{\mathrm{miss}}}|$	>0.5	
$|\Delta\phi_{jj}|$	<1.5	
$\eta_1 \cdot \eta_2$	<0	
$|\Delta\eta_{jj}|$	>4.0	>1.0
m_{jj}	>1.3 TeV	> 200 GeV (binned)

TABLE I. Summary of the main kinematic requirements in the signal regions in Ref. [41].

cut-and-count analysis and 0.28 for the shape analysis which are both weaker than the upper limit $\mathrm{BR}_{h\to\mathrm{inv}}^{\mathrm{max}} = 0.24$ used as a hard cut in our scan (see section III B). This constraint is only applicable to parameter points in the IDM for which $m_H < m_h/2$. However, points with heavier scalars would also predict additional signal events in the above analysis due to processes with off-shell h production ($pp \to h^*jj \to HHjj$) and contributions from decay chains with hadronically decaying final state particles (e.g. $pp \to H^\pm H \to jjHH$). We *recast* the above mentioned VBF analysis in the context of these processes to potentially extract additional constraints applicable to regions with larger values of m_H.

B.   Simulation and Validation of the VBF Channel

In this work, we concentrate on the above VBF search which has been implemented within the `CheckMATE` [43, 44] framework. `CheckMATE` uses simulated event files for any BSM model, applies detector efficiencies and follows the event selection procedure of the implemented BSM searches from ATLAS and CMS to determine if any resulting signal prediction would violate the corresponding experimental bound.[11] Validation has been performed by reproducing the quoted numbers expected from the Standard Model Higgs boson with 100% invisible branching ratio. Following the procedure described in the experimental publication, we use the POWHEG-Box [100–103] for simulating Monte-Carlo events at next-to-leading order in QCD and subsequently interface it to `Pythia 6.4.21` [104] to account for parton showering and hadronization of the final state. We perform the simulation separately for vector-boson-fusion (vbf) and gluon-initiated final states (ggf) which may also pass the aforementioned cuts.

As we are bound to leading order Monte Carlo tools for the simulation of the IDM, we additionally generate tree-level parton events with `MG5_aMC@NLO` [105] showered with `Pythia 8.219` [106] — the same tools which we use for our subsequent IDM analysis — to quantify the effect of an LO-only simulation. Both event samples are processed with `CheckMATE` and the resulting signal predictions are shown in table II.

As can be seen, our setup reproduces the experimentally quoted results sufficiently well within the experimentally quoted error margin when using simulated events generated with an NLO-QCD Monte Carlo event generator. A leading-order Monte Carlo analysis, in comparision, significantly underestimates the signal prediction with a nearly constant ratio of ≈ 1.7 across all signal regions.

The numbers in Tab. II can be used to derive upper limits on the invisible branching ratio of the Standard Model Higgs. For this purpose we employ a profile likelihood ratio test paired with the CLs prescription. For the shape analysis, we make use of the full background covariance matrix provided in Ref. [41]. As no such detailed information is provided for the signal, we conservatively assume that it is fully correlated across all bins. Our resulting distribution for the test statistics is shown in Fig. 1. We are able to reproduce this distribution sufficiently well by either using our

———

[11] For more information about how `CheckMATE` works we refer to the corresponding manuals in Refs. [43, 44]. We implemented the above mentioned VBF search using the `AnalysisManager` tool described in Ref. [99].

Region	Data	Background	SM prediction with BR($h \rightarrow$invisible) = 100 %			
		CMS	CMS	Our Simulation		
				`Powheg-Box`	`MG5_aMC@NLO`	Ratio
CutandCount	2053	1779 ± 96	851 ± 148	758	468	1.6
$m_{jj} \in [200, 400]$ GeV	16177	14878 ± 566	591 ± 285	708	390	1.8
$m_{jj} \in [400, 600]$ GeV	10008	9401 ± 387	571 ± 232	664	374	1.8
$m_{jj} \in [600, 900]$ GeV	7277	6658 ± 271	566 ± 172	737	433	1.7
$m_{jj} \in [900, 1200]$ GeV	3138	2994 ± 144	472 ± 131	483	293	1.7
$m_{jj} \in [1200, 1500]$ GeV	1439	1283 ± 69	307 ± 64	314	202	1.7
$m_{jj} \in [1500, 2000]$ GeV	911	834 ± 51	344 ± 83	319	203	1.6
$m_{jj} \in [2000, 2750]$ GeV	408	358 ± 29	228 ± 40	218	126	1.8
$m_{jj} \in [2750, 3500]$ GeV	87	73.8 ± 9.4	90.3 ± 18.8	80.1	48.8	1.7
$m_{jj} > 3500$ GeV	29	30.3 ± 7.4	37.4 ± 9.1	38.2	19.9	1.9

TABLE II. Observed and expected number of events for all regions listed in Table I. SM predictions are determined for an entirely invisibly decaying Standard Model Higgs boson with $m_h = 125$ GeV produced both in Vector Boson Fusion and Gluon Fusion. CMS numbers are taken from Ref. [41] and compared to our numbers determined with our analysis implementation in `CheckMATE`, using both the LO-QCD generator `MG5_aMC@NLO` and the NLO-QCD Monte Carlo simulation `Powheg-Box`. Uncertainties quoted for CMS include both statistical and systematical uncertainties.
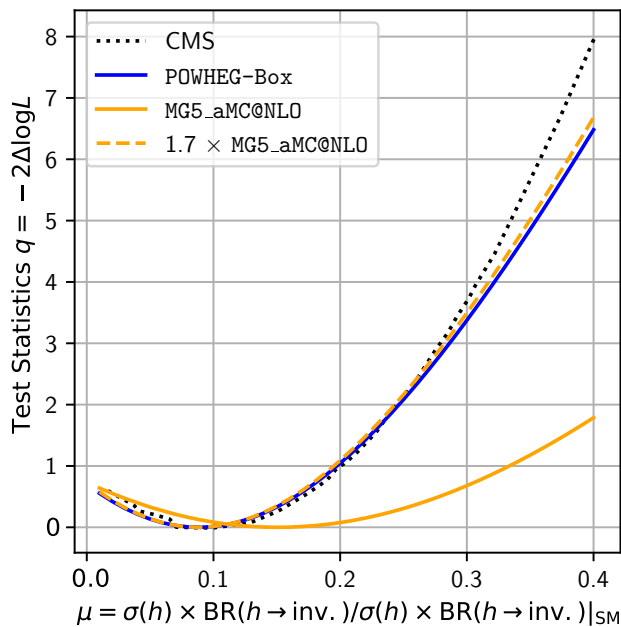

FIG. 1. Comparision of the log-likelihood-ratio, using the numbers in Tab. II.

results determined with `POWHEG` or by rescaling the results of our leading-order simulation with a constant K-factor of 1.7.

From our validation and the comparision of the above results using LO and NLO simulation, we conclude that a leading order simulation of the IDM signal is expected to systematically underestimate the correct number. However, a full next-to-leading order simulation of the off-shell VBF channel within the IDM is beyond the scope of this work.

We determine results for the IDM at leading order. To be more precise, we simulate

$$pp \to HHjj \tag{23}$$

event samples for the IDM within `MG5_aMC@NLO` and `Pythia 8.219` by making use of the UFO model description of Ref. [19]. We here do not specify intermediate states, i.e. on parton level all processes leading to the final state given in Eqn. (23) have been taken into account. Besides VBF production of a SM-like scalar with invisible decays, this also includes e.g. HA or $H^\pm H$ pair-production with the subsequent decay $A \to Hjj$, $H^\pm \to Hjj$ or vector boson scattering processes with dark scalars in the $t-$channel. Relative contributions of the latter to the total cross section become sizeable as $|\lambda_{345}| \to 0$. We include an invariant mass cut $m_{jj} \geq 130$ GeV and a pseudorapidity difference cut $\Delta\eta_{jj} \geq 0.5$ with $\eta_1\eta_2 < 0$ in our parton event generation. Note that these are weaker than the signal region cuts in Tab. I.

From our above findings, we expect our resulting bounds to be conservative. However, motivated from the results in Table II we also discuss the limits we obtain if our signal prediction is upscaled with the global K-factor of 1.7 motivated before to illustrate the potential impact of next-to-leading-order QCD effects.

C.   Features and Setup of the Monojet analysis

Nearly any particle model with a dark matter candidate H predicts the standard monojet signature $pp \to HHj$ for the LHC where the jet may originate from initial state radiation or, in some specific models other than ours, from the hard vertex. It is therefore to be expected that this channel is sensitive to the IDM in which H plays the role of the dark matter candidate. A detailed analysis of this channel can be found in Ref. [32]. However, as has for example been shown in Ref. [107] in the context of a different model with similar topology, the vector boson fusion channel is expected to be significantly more sensitive than the monojet search. We reproduce this finding later.

The analysis of the monojet channel is performed within `CheckMATE`, similarly to the analysis above. As this analysis had already been implemented in the public code, we do not provide a separate validation here.[12] We simulate the partonic process $q\bar{q}, gg \to HHj$ with `MG5_aMC@NLO` and apply a p_T cut of 200 GeV on the leading jet, in accordance with the signal region requirement $p_T^j \geq 250$ GeV of this analysis.

V.   PARAMETER SPACE CONSTRAINTS

In this section, we present the constraints resulting from the our recast of the searches for an invisibly decaying Higgs in both the vector boson fusion and the monojet channel. We initially consider parameter points which have passed all bounds presented in section III, *apart from* the constraints imposed by dark matter bounds, i.e. dark matter relic density as well as direct detection, cf. Eqs. (19) and (20). This approach allows for an investigation of the complementary between astrophysical and collider searches for this model.

Collider Constraints

We now demonstrate the effect of including the searches in Refs. [41], [42] as introduced in the previous section. Our results are shown in Fig. 2 (left) where we only consider points which pass all prior constraints discussed in Sec. III.[13] The general influence of these constraints has been discussed in detail in Refs. [22, 45] and will not be

---

[12] Validation material for this analysis can be found on the official `CheckMATE` website, `https://checkmate.hepforge.org/AnalysesList/ATLAS_13TeV.html`.

[13] We note that the density of points has no theoretical meaning but is just a reflection of a bias in the generation of theoretical parameter tuples.
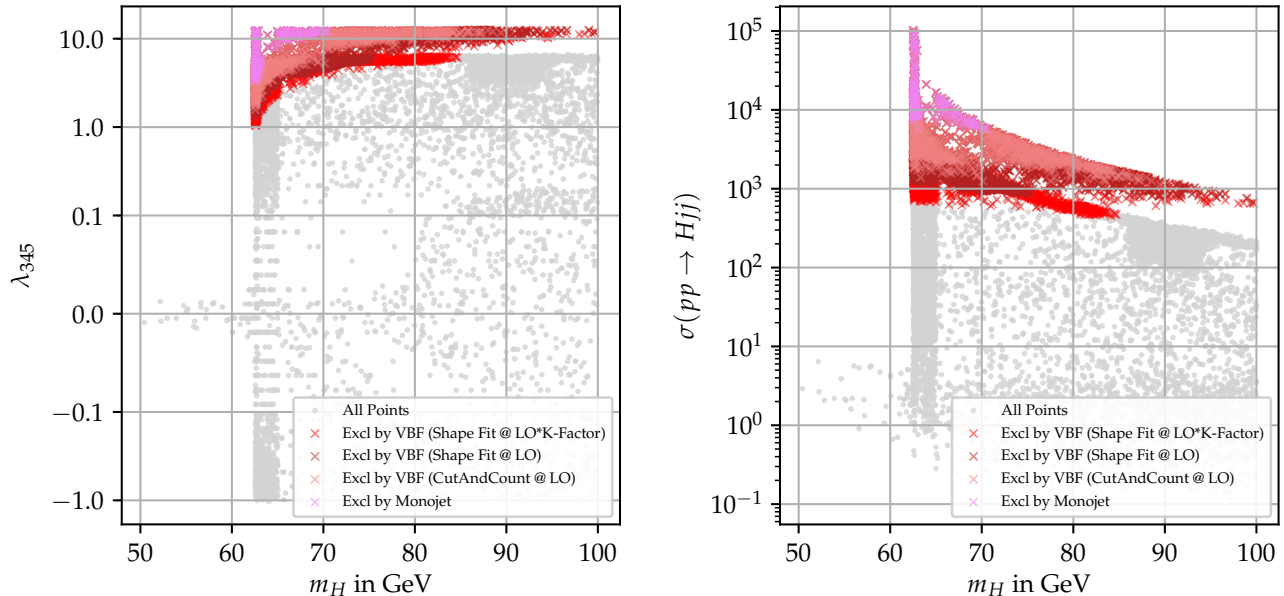
FIG. 2.   Allowed and excluded points after consideration of VBF and monojet analysis but without dark matter relic density and direct detection constraints. VBF results are shown using different categories, see in-text discussion. *Left:* Results in (m_H, λ_{345}) parameter plane. *Right:* Results in m_H-σ plane where σ is the LHC VBF production cross section at 13 TeV including the partonic cuts given in Sec. IV B.

repeated here. For values $m_H \leq m_h/2$, it is especially the branching ratio limit on $h \to$ invisible which leads to the tight constraint $|\lambda_{345}| \lesssim 0.03$. For larger m_H values, however, λ_{345} can reach values up to the perturbativity limit 4π which has been imposed as a hard upper cut in the scan setup. Note that we have explicitly verified that the small stripe for $m_H > 80$ GeV, $\lambda_{345} > 6$ contains no viable parameter points as it is excluded by combining perturbativity requirements with limits on the electroweak oblique parameters and $R_{\gamma\gamma}$, see e.g. discussion in Ref. [22].

We separately indicate which points are respectively excluded by the monojet and by the VBF search. For the latter, we explicitly distinguish the following exclusion categories.

- In `CutAndCount@LO`, we only determine the number of signal events in the cut-and-count signal region of Ref. [41] and use a single-bin likelihood ratio test to determine whether it is compatible with the numbers of observed and expected Standard Model events, see Tab. II.

- In `Shape Fit@LO` we determine the number of signal events in all m_{jj} binned signal regions of Tab. II and use a joint likelihood, including the background correlation matrix provided in Ref. [41], to determine the overall p-value.

- Whilst for the above two approaches we use the signal numbers as determined with the Monte Carlo generator `MG5_aMC@NLO` at leading order, for `Shape Fit@LO*K- Factor` we multiply all numbers with the constant K-factor of 1.7, c.f. discussion in Sec. IV B.

According to our SM validation, we expect `LO` results to significantly underestimate the number of signal events and therefore lead to conservative bounds. Showing the results including the K-factor determined from our SM validation renders an estimate of the impact of higher-order QCD contributions.

In general, we observe that a significant fraction of points can be constrained by the two collider searches considered in this work. As foreseen in Sec. IV C, the monojet channel shows a significantly reduced sensitivity as compared to
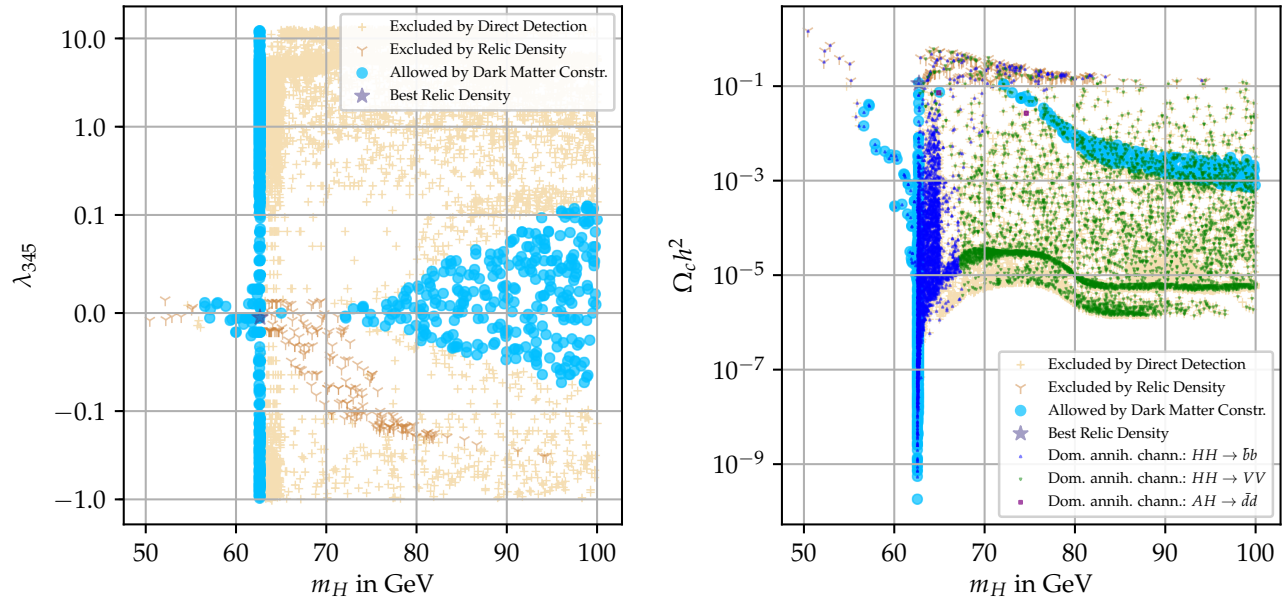
FIG. 3. Parameter space after including dark matter relic density and direct detection constraints. *Left:* allowed and forbidden regions in the (m_H, λ_{345}) plane. *Right:* Constraints in the $(m_H, \Omega_c h^2)$ plane. On the right plot, we also show the dominant annihilation cross section for each parameter point. The "Best Relic Density" point yields $\Omega_c h^2 = 0.1141$ which is the closest to the nominal Planck value, c.f. Eq. (18), out of all tested points.

the VBF search.[14] Though both channels suffer largely from SM QCD background sources, the VBF channel can make more precise predictions on the extected kinematics of the jets in the final state. This ultimatively allows for a higher signal-to-background ratio in the signal bins and thus results in a better sensitivity for many models in which both channels are present simultaneously.

Whilst monojet studies alone are sensitive to values of λ_{345} down to 2.5 and m_H masses in the range $[m_h/2$ - 70] GeV, we observe VBF reinterpretations to constrain λ_{345} down to 1 and extend the sensitivity range on m_H values up to the maximum of 100 GeV we consider. No parameter point with $m_H < m_h/2$ can be constrained as the small values of λ_{345} predict a far too small cross section. This can also be seen on the right of Fig. 2 where we show our bounds in terms of the VBF cross section, including the partonic cuts described in Sec. IV B. In fact, this region is largely constrained by the cut on $\mathrm{BR}_{h\to\mathrm{inv}} \leq 0.24$ which we discuss in Sec. III B. As the VBF channel consists of one sub-measurement of this observable, it is evident that it cannot provide additional, stronger bounds than the one on the invisible branching ratio which has been used to generate our parameter samples.

Note that, though the bound is clearly very much dependent on the size of the cross section, we observe on the right of Fig. 2 that it is not flat in the m_H-σ-plane. This can be explained by differences in the signal efficiency from additional, small IDM contributions like $pp \to H^\pm H, H^\pm \to jjH$ which, in addition to m_H, also depend on the masses of the other inert scalars. The fact that the bound is not only dependent on the total cross section shows the importance of dedicated Monte Carlo recast analyses including off-shell effects.

---

[14] Our results appear to be compatible with former monojet sensitivity studies shown in Ref. [32] which show no sensitivity for a benchmark point with $\lambda_{345} = 1.7$ using an older version of the monojet search with only 10% of the integrated luminosity that our analysis uses.
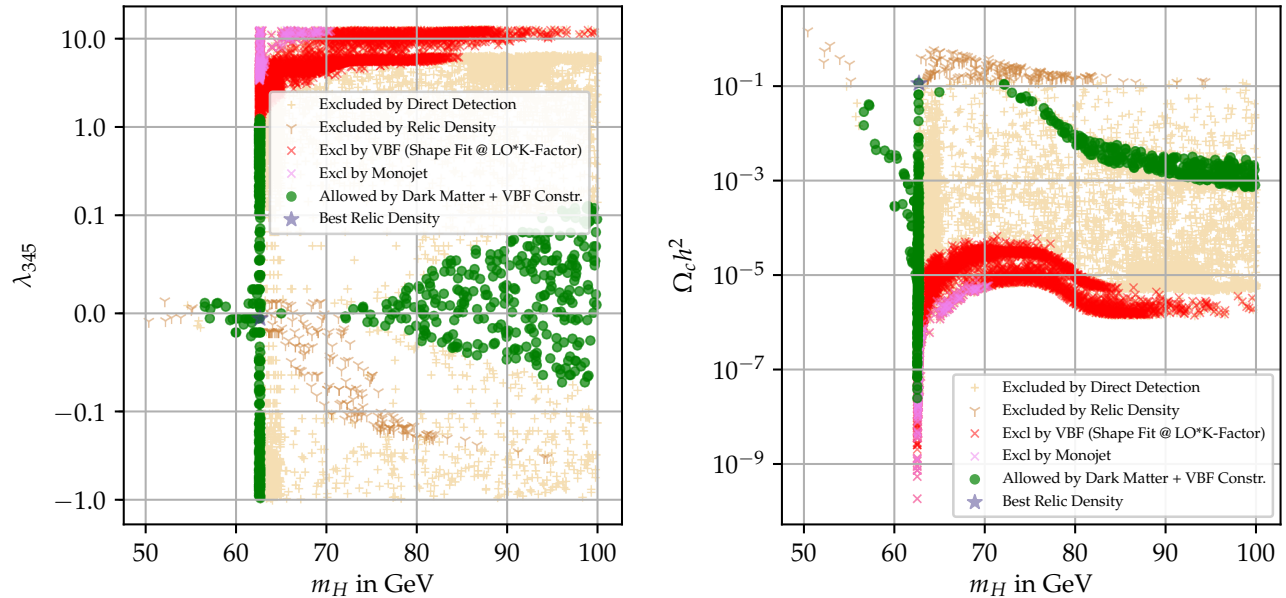
FIG. 4.   Parameter space after including all constraints (see also explanations below Fig. 3)

Dark Matter Constraints

We now impose the dark matter constraints specified by Eqs. (19) and (20) on the parameter space. As has been noted in Refs. [23, 45], it is especially direct detection constraints which have improved by an order of magnitude with respect to the previous study in Ref. [22] which used the 2013 LUX results, c.f. Ref. [108]. The parameter space is severely constrained, as is demonstrated in Fig. 3 where we now discuss the dark matter bounds on our parameter space without applying the VBF/Monojet limits. Fig. 3, left, shows the results in the m_H-λ_{345} plane and Fig. 3, right, displays the relic density abundance $\Omega_c h^2$ in dependence on m_H. The second figure also labels the dominant annihilation channel for each tested parameter point as determined via `MicrOmegas`.[15] We also indicate the point in our sample whose predicted value of $\Omega_c h^2 = 0.1141$ is closest to the Planck value in Eq. (18). This point yields 95 % of the required cold dark matter relic density. Especially for masses $m_H \geq 63$ GeV, we find that $|\lambda_{345}|$ needs to be small, $\lesssim 0.14$ for $m_H \approx 100$ GeV and even tighter bounds for lighter m_H. However, there also exists a small mass window, $m_H \in [m_h/2; 63\,\text{GeV}]$ which allows for values of λ_{345} up to our theoretical limit of 4π. As can be seen in the right of Fig. 3, this region predicts particularly small values of Ω and therefore avoids both relic density and direct detection constraints, see Eq. (20). When the intermediate SM-like Higgs boson h is on shell, the annihilation cross section $HH \to b\bar{b}$ is enhanced and results in a considerably smaller dark matter relic density (see also discussion in [22, 98]).

---

[15] For relatively small mass differences between the two dark neutral scalars A and H, typically of a few GeV, the co-annihilation channel $AH \to d\bar{d}$ becomes dominant. As this requires a relatively fine-tuned scenario, our scan only tested 2 such points. See also the discussion in [22, 98].

Finally, in Fig. 4, we show the allowed and excluded parameters m_H and λ_{345}, as well as $\Omega_c h^2$, after all the above constraints are taken into account. As can be seen, collider results start to close the annihilation window, $m_H \approx m_h/2$, which could bypass direct detection constraints by significantly reducing the predicted relic density $\Omega_c h^2$. Here, only collider searches can put bounds on values of λ_{345} above 1. However, this only constrains points with very small $\Omega_c h^2$; therefore still a large number of points in this kinematic window remain allowed, including our "Best Relic Density" point discussed above. Moreover, for values of m_H significantly larger than $m_h/2$, collider limits may yield important bounds. However in the IDM we find that these are always already excluded by direct detection limits.

It must be noted, though, that if the lightest IDM scalar H couples to an extended dark sector and in fact decays to the actual, lighter dark matter candidate, relic density and direct detection constraints can change significantly while the above collider bounds are typically unaffected if H has further invisible decays (see e.g. Ref. [109] in the context of the so-called "radiative seesaw model" which extends the IDM with an additional Majorana neutrino dark matter candidate). Therefore, even though in the pure IDM collider limits seem to hardly provide additional sensitivity compared to direct detection limits, they still constitute an important analysis channel complementary to dark matter findings.

VI.   NULL RESULTS FROM OTHER RECAST CHANNELS

The above VBF and monojet analyses focus on the dark matter candidate H and thus are largely independent of the masses $m_A, m_{H^\pm}$ of the other two scalar particles and their decay rates. However, within our scan we only considered dark masses $\leq 500\,\text{GeV}$. Thus the question may arise if any of the many other BSM searches performed by ATLAS and CMS could result in additional, stronger constraints than the one considered.

In Fig. 5 we display the masses $m_{H^\pm}, m_A$ for all points that are allowed by our previous scan. Similar to findings in Refs. [22, 45], we observe a relatively strong mass degeneracy of these two heavier dark scalars. We also show the corresponding mass differences $m_A - (m_H + m_Z)$ and $m_{H^\pm} - (m_H + m_{W^\pm})$ of the allowed points. This quantity can be used to roughly estimate the kinematics of the expected decays for the heavier scalars A and $H^\pm$. For mass differences larger/smaller than 0, we expect on/off-shell decays into gauge bosons, e.g. $A \to HZ^{(*)}$, with 100% branching ratio due to the absence of any other lighter D-odd particles. We focus on the leptonic decay modes of the gauge bosons as within the analyses we consider, hadronic modes are typically harder to distinguish from QCD background.

The larger the mass difference, the more energy is expected to be passed on to the daughter particles. A high-momentum H in the final state is expected to produce missing transverse momentum (MET) in the event, a key observable for BSM signals. However, as can be seen in Fig. 5, viable IDM points only predict large mass differences for parameter points if also the absolute masses of m_A and $m_{H^\pm}$ are increased. Points with a large mass splitting and good final state efficiency therefore in turn suffer from respectively smaller expected LHC production cross sections. Therefore, a dedicated Monte Carlo recast procedure is necessary in order to identify which points are subject to constraints from direct LHC searches.

Fortunately, `CheckMATE` bears the great advantage of being capable of quickly testing many such analyses simultaneously. We hence used it to perform a more inclusive scan of other potentially relevant final states. To be more precise, we considered the two body final states

$$pp \to HA, \ HH^\pm, \ AA, \ AH^\pm \text{ and } H^+H^-. \tag{24}$$

We simulated all above processes in `MG5_aMC@NLO`, including a full consideration of the 2- and 3-body decays of A and $H^\pm$ into H and a set of Standard Model particles. These events are subsequently tested against all 13 TeV analyses implemented in `CheckMATE` — a list is given in appendix B.

It turns out that none of our $> 10,000$ considered parameter tuples appear to be excluded by any search other than the already considered VBF and monojet channels.
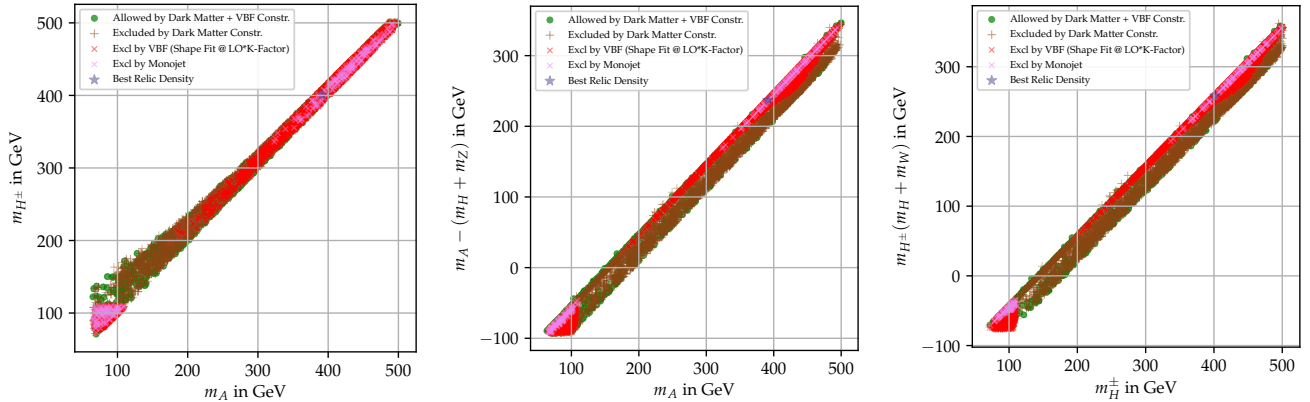
14

FIG. 5. Allowed combinations of the scalar masses $m_{H^\pm}$, m_A and m_H which are relevant for collider analysis of the channels $pp \to HA$ and $pp \to H^\pm A$.

Note that though we inclusively test all possible final states, the highest sensitivity is expected from leptonic final states, i.e.

$$pp \to AH, A \to Z^{(*)}_{\text{lep}} H \tag{25}$$

$$pp \to AH^\pm, A \to Z^{(*)}_{\text{lep}} H, H^\pm \to W^\pm_{\text{lep}} H. \tag{26}$$

The first signature is covered by Ref. [110] which searches for final state with invisible particles produced in association with a leptonically decaying Z-boson.[16] We refer to this analysis as "2ℓ" in the following. In contrast, the second example signature is covered[17] by Ref. [111] — for short "3ℓ" in the following text — which looks for various leptonic (and hadronic) final states in supersymmetric electroweakino production, i.e. $\tilde{\chi}_1^+ \tilde{\chi}_1^-$ and $\tilde{\chi}_1^\pm \tilde{\chi}_2^0$. The expected final state for mixed chargino-neutralino production is experimentally identical to the aforementioned $AH^\pm$ decay chain and thus may be used to constrain the IDM.

To understand the reason for the non-sensitivity of current electroweakino searches, we show our results for the AH-channel and the $H^\pm A$ channel in Fig. 6. In each subplot, we show the respective r-value of the analysis, defined as the ratio of the signal predicted by `CheckMATE` for the most sensitive signal region and the model-independent upper limit on a signal in this signal region. Most importantly, r scales with the predicted signal cross section and a value of $r \geq 1$ can be interpreted as a model point excluded at 95% confidence level.

For the x-axis, we respectively show the mass difference of a heavy inert scalar, A or $H^\pm$, and the summed masses of the two particles it decays into, e.g. $m_A - (m_Z + m_H)$ for $A \to ZH$. As explained before, the mass difference provides an estimate for the typical energy given to the leptons and to the dark matter candidate H in the form of MET.

As can be seen from the figures, there is no 1:1 correspondence between the aforementioned mass difference and the model exclusion. This is obvious since the limit also depends on the absolute mass scales which for a given mass difference can change within ± 50 GeV, c.f. Fig. 5. However, one observes an overall rise-and-fall of the sensitivity and a global maximum near $m_A - (m_H + m_Z) \approx 50$ GeV and $m_{H^\pm} - (m_H + m_{W^\pm}) \approx 125$ GeV. This structure can be explained from our discussion at the beginning of this section: The larger the mass difference, the higher the expected

---

[16] Note that this final state has been analysed before in Ref. [20] using Run 1 dilepton final states. However, the parameter regions they consider are excluded after applying constraints from dark matter relic density and the invisible width of the SM Higgs boson.

[17] Note that `Checkmate`, and therefore also our analysis, makes use of preliminary results in Ref. [111] which were subsequently updated by a full publication in Ref. [112]. However, the published results are identical to those in the preliminary conference note.
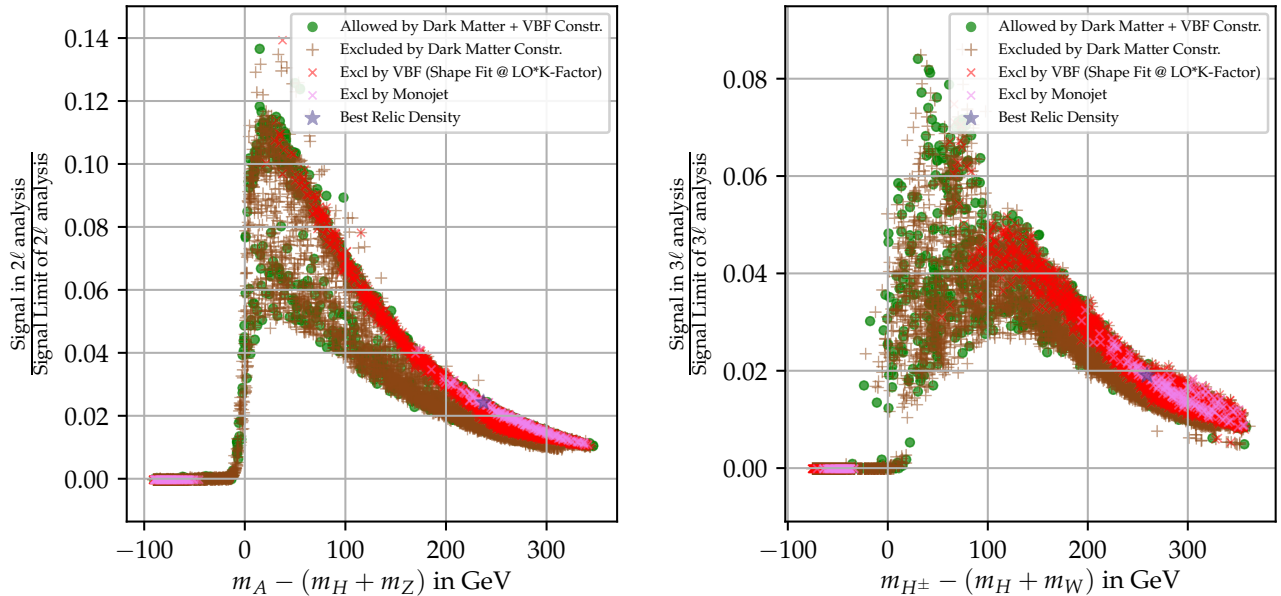
FIG. 6. Results for our LHC reinterpretation of SUSY electroweakino results on the masses of the IDM. The x-axis shows mass differences which are strongly correlated to the MET distribution in the final state. The y-axis denotes the r-value, defined as the ratio of the signal prediction divided by the 95 % confidence limit on the signal.

amount of lepton p_T and MET in the final state becomes and so the overall signal efficiency increases. However, in order to obtain higher mass differences, electroweak precision constraints require larger masses for A and $H^\pm$ and thus generally predicts smaller cross sections for viable IDM realisations. Hence, large mass differences simultaneously increase the final state efficiency and decrease the expected cross section. For the 2ℓ analysis, this results in a peak at a mass difference of approximately 30 GeV which is related to the minimum p_T cut on the signal leptons and the MET requirement of this analysis. For the 3ℓ analysis, no overall peak can be determined as the final state consists of two separate decay chains whose kinematic configurations simultaneously depend on m_A and $m_{H^\pm}$. Still, a similar behaviour can be observed.

However, as can be seen, the peak values for both analyses still only predict at most 15 % of the required number of events for the analyses to be sensitive to the signal. Hence, we conclude that electroweakino searches are currently not sensitive to the IDM and from a statistical point of view, this may only change in the high luminosity limit of LHC 14. Still, the presented analysis only shows reinterpreted results motivated from different signal models and therefore not necessarily optimised towards the IDM. It may therefore be possible that a collider search specifically targeting the IDM may improve upon the results determined here via reinterpretation.

As an example, Fig. 7 illustrates how many events with leptonic final states are respectively expected from the processes in Eqs. (25), (26), *without* applying any event selection cuts. Note that for a signal to be observable e.g. in the 2ℓ analyses one requires at least 200 events *after* requiring the missing transverse momentum to be at least 90 GeV. It becomes apparent from Fig. 7 that a considerably softer cut on MET would significantly increase the number of expected signal events after cuts within the IDM. A full sensitivity study would however require the re-evaluation of SM background after modifying cuts. Such an analysis would provide important complementary information since, as can be seen from the different categories shown in Fig. 6, many points in the peak region of the direct search are neither excluded by the VBF channel nor by dark matter direct detection.
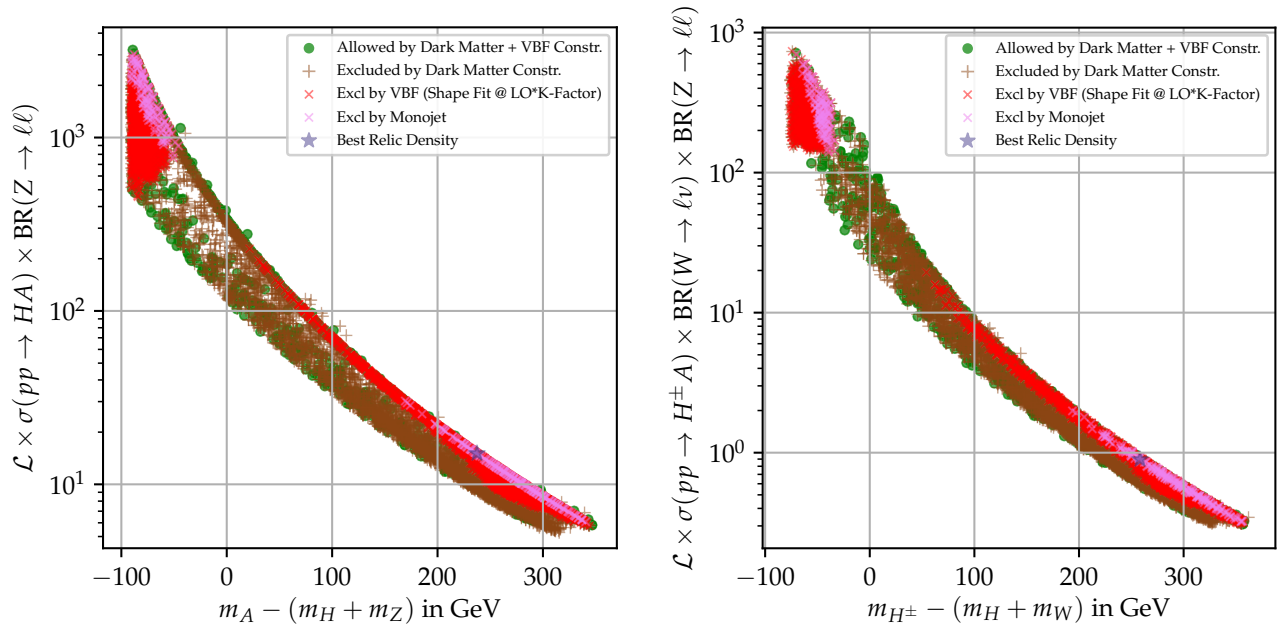
FIG. 7. Predicted number of events in the $2\ell/3\ell$ channels. The x-axis shows mass differences as in Fig. 6. The y-axis denotes the product of integrated luminosity, total production cross section and leptonic branching ratio of the expected gauge boson(s) in the final state.

VII. CONCLUSIONS

In this paper, we have considered the Inert Doublet Model, a two Higgs doublet model with a discrete Z_2 symmetry containing a scalar dark matter candidate. We have included all current theoretical and experimental collider constraints on this model as discussed in Ref. [45]. Concentrating on the region where $m_H \leq 100\,\text{GeV}$, we have investigated limits on the models' parameter space from a recast of recent LHC search where the invisibly decaying SM Higgs is produced either in vector boson fusion, Ref [41], or in association with a hard jet, Ref. [42]. For this, we have implemented the above searches in the collider phenomenology tool `CheckMATE` and tested their sensitivity compared to constraints from dark matter and direct detection.

We observe that the VBF channel outperforms the monojet analysis and is sensitive to a large fraction of IDM parameter space and a proper recast of this analysis results in important bounds on the IDM model. Our search can significantly constrain a specific window in parameter space with dark matter masses $\sim 62 - 63\,\text{GeV}$ which evades dark matter limits due to an enhanced annihilation rate and leads to a significantly reduced relic abundance. This softens constraints from direct detection experiments like `XENON1T`. For larger masses, the VBF channel still provides relevant bounds which however do not improve direct detection limits within the pure IDM. The latter, however, could be avoided by coupling the lightest IDM scalar to a lighter dark matter sector which would have nearly no consequence for our presented collider analysis.

As no direct search for IDM scalars exist, we further reinterpret searches for BSM particles with the same experimental signature and conclude that these do not put further constraints on the IDM. We trace this back to the effect that either the cross section is too small or the mass splitting is not large enough to predict sufficiently high-energetic final state particles. In this context, it might be interesting to pursue whether a dedicated search for the inert scalars could enhance the expected LHC sensitivity and eventually provide complementary information to the VBF channel and dark matter direct detection, especially about the other scalar masses of the dark sector.

Appendix A: IDM Feynman rules and other relations

The parameters m_{22}^2, λ_3, λ_4, λ_5 can be re-expressed in terms of our input parameters:

$$m_{22}^2 = \lambda_{345}\, v^2 - 2\, m_H^2,$$
$$\lambda_3 = \lambda_{345} - \frac{2}{v^2}\left(m_H^2 - m_{H^\pm}^2\right),\ \lambda_4 = \frac{m_A^2 + m_H^2 - 2\, m_{H^\pm}^2}{v^2},$$
$$\lambda_5 = \frac{m_H^2 - m_A^2}{v^2}.$$

For completeness, we list the relevant Feynman rules of the IDM scalars in Tables III,IV and V, omitting Goldstone modes as we are working in the unitary gauge at tree level. Note that the second, inert doublet neither participates in electroweak symmetry breaking nor in the generation of fermion masses. Hence, the couplings of the SM-like Higgs h to electroweak gauge bosons as well as fermions are given by their SM values, see e.g. [113], with the convention $g_{hW_\mu^+ W_\nu^-} = ie^2 v/2s_W^2 g_{\mu\nu}$.

vertex	coupling
hHH	$\lambda_{345}\, v$
hAA	$\bar{\lambda}_{345}\, v$
hhh	$3\,\lambda_1\, v$
$h\, H^+\, H^-$	$\lambda_3\, v$

TABLE III. Triple scalar vertices

vertex	coupling
$hhhh$	$3\,\lambda_1$
$H^+\, H^+\, H^-\, H^-$	$2\,\lambda_2$
$HHAA$	λ_2
$HHHH$	$3\,\lambda_2$
$AAAA$	$3\,\lambda_2$
$H^+ H^-\, AA$	λ_2
$H^+ H^- HH$	λ_2
$hh H^+ H^-$	λ_3
$hhHH$	λ_{345}
$hhAA$	$\bar{\lambda}_{345}$

TABLE IV. Quartic scalar vertices

vertex	coupling
$H^-\, H^+\, \gamma$	$i\, e$
$H^-\, H^+\, Z$	$i\,\frac{g}{2}\,\frac{\cos\left(2\theta_W\right)}{\cos\theta_W}$
$H\, H^\pm\, W^\mp$	$\mp\, i\,\frac{g}{2}$
$A\, H^\mp\, W^\pm$	$-\frac{g}{2}$
$H\, A\, Z$	$-\frac{g}{2\cos\theta_W}$

TABLE V. Gauge-scalar vertices

Appendix B: List of Applied CheckMATE Analyses

Table VI gives the full list of used `CheckMATE` analyses with a centre-of-mass energy of $\sqrt{s} = 13$ TeV. The first column shows the `CheckMATE` idenitifer, the second the purpose for which the analysis was designed for. The last three columns show the number of signal regions in the corresponding analysis (marked #SR), the integrated luminosity for that analysis and the reference to the publication or conference notes from the experimental collaborations. We mark

`CheckMATE identifier`	Search designed for	#SR	L_{int}	Ref.
`atlas_1602_09058`	Supersymmetry in final states with jets and two SS leptons or 3 leptons	4	3.2	[114]
`atlas_1604_01306`	New phenomena in events with a photon and $\not\!\!E_T$	1	3.2	[115]
`atlas_1604_07773`	New phenomena in final states with an energetic jet and large $\not\!\!E_T$	13	3.2	[116]
`atlas_1605_03814`	$\tilde{q}$ and $\tilde{g}$ in final states with jets and $\not\!\!E_T$	7	3.2	[117]
`atlas_1605_04285`	Gluinos in events with an isolated lepton, jets and $\not\!\!E_T$	7	3.3	[118]
`atlas_1605_09318`	Pair production of $\tilde{g}$ decaying via $\tilde{t}$ or $\tilde{b}$ in events with b-jets and $\not\!\!E_T$	8	3.3	[119]
`atlas_1606_03903`	$\tilde{t}$ in final states with one isolated lepton, jets and $\not\!\!E_T$	3	3.2	[120]
`atlas_1609_01599`	Measurement of ttV cross sections in multilepton final states	9	3.2	[121]
`atlas_conf_2015_082`	Supersymmety in events with leptonically decaying Z, jets and $\not\!\!E_T$	1	3.2	[122]
`atlas_conf_2016_013`	Vector-like t pairs or 4 t in final states with leptons and jets	10	3.2	[123]
`atlas_conf_2016_050`	$\tilde{t}$ in final states with one isolated lepton, jets and $\not\!\!E_T$	5	13.3	[124]
`atlas_conf_2016_054`	$\tilde{q}$, $\tilde{g}$ in events with an isolated lepton, jets and $\not\!\!E_T$	10	14.8	[125]
`atlas_conf_2016_076`	Direct $\tilde{t}$ pair production and DM production in final states with 2ℓ	6	13.3	[126]
`atlas_conf_2016_078`	Further searches for $\tilde{q}$ and $\tilde{g}$ in final states with jets and $\not\!\!E_T$	13	13.3	[127]
`atlas_conf_2016_096`	Supersymmetry in events with 2ℓ or 3ℓ and $\not\!\!E_T$	8	13.3	[128]
`atlas_conf_2017_022`	$\tilde{q}$, $\tilde{g}$ in final states with jets and $\not\!\!E_T$	24	36.1	[129]
`atlas_conf_2017_039`	**Electroweakino production in final states with 2 or 3 leptons**	37	36.1	[111]
`atlas_conf_2017_040`	**Dark Matter or invisibly decaying h, produced in associated with a Z**	2	36.1	[130]
`atlas_conf_2017_060`	**New phenomena in final states with an energetic jet and large $\not\!\!E_T$**	13	36.1	[131]
`cms_pas_sus_15_011`	New physics in final states with an OSSF lepton pair, jets and $\not\!\!E_T$	47	2.2	[132]
`cms_pas_hig_17_023`	**Search for invisible decays of h produced through VBF**	10	36.1	[41]

TABLE VI. Full list of all $\sqrt{s} = 13$ TeV `CheckMATE` analyses used for this study. Entries in boldface are relevant for the model studied in this work and are discussed in the main text. The column labelled #SR yields the number of signal regions. Entries for the integrated luminosities L_{int} are given in fb^{-1}.

all analyses discussed in our main discussion in boldface. Note that `Checkmate` regularly implements preliminary results published as conference notes by the experimental LHC collaborations and use the corresponding `conf-note` identifiers. Often, these are published at a later stage by the collaborations without any changes to analysis procedure or results. More details on the individual analyses can be found in their respective references and corresponding validation material, if not provided in this work, can be found on `http://checkmate.hepforge.org`.

[1] Nilendra G. Deshpande and Ernest Ma. Pattern of Symmetry Breaking with Two Higgs Doublets. *Phys. Rev.*, D18:2574, 1978.

[2] Qing-Hong Cao, Ernest Ma, and G. Rajasekaran. Observing the Dark Scalar Doublet and its Impact on the Standard-Model Higgs Boson at Colliders. *Phys. Rev.*, D76:095011, 2007, 0708.2939.

[3] Riccardo Barbieri, Lawrence J. Hall, and Vyacheslav S. Rychkov. Improved naturalness with a heavy Higgs: An Alternative road to LHC physics. *Phys.Rev.*, D74:015007, 2006, hep-ph/0603188.

[4] Laura Lopez Honorez, Emmanuel Nezri, Josep F. Oliver, and Michel H.G. Tytgat. The Inert Doublet Model: An Archetype for Dark Matter. *JCAP*, 0702:028, 2007, hep-ph/0612275.

[5] Laura Lopez Honorez and Carlos E. Yaguna. The inert doublet model of dark matter revisited. *JHEP*, 1009:046, 2010, 1003.3125.

[6] Ethan M. Dolle and Shufang Su. The Inert Dark Matter. *Phys.Rev.*, D80:055012, 2009, 0906.1609.

[7] Dorota Sokolowska. Dark Matter Data and Quartic Self-Couplings in Inert Doublet Model. *Acta Phys.Polon.*, B42:2237, 2011, 1112.2953.

[8] I.F. Ginzburg, K.A. Kanishev, M. Krawczyk, and D. Sokolowska. Evolution of Universe to the present inert phase. *Phys.Rev.*, D82:123533, 2010, 1009.4593.

[9] Thomas Hambye and Michel H.G. Tytgat. Electroweak symmetry breaking induced by dark matter. *Phys.Lett.*, B659:651–655, 2008, 0707.0633.

[10] Talal Ahmed Chowdhury, Miha Nemevsek, Goran Senjanovic, and Yue Zhang. Dark Matter as the Trigger of Strong Electroweak Phase Transition. *JCAP*, 1202:029, 2012, 1110.5334.

[11] Debasish Borah and James M. Cline. Inert Doublet Dark Matter with Strong Electroweak Phase Transition. *Phys.Rev.*, D86:055001, 2012, 1204.4722.

[12] Grzegorz Gil, Piotr Chankowski, and Maria Krawczyk. Inert Dark Matter and Strong Electroweak Phase Transition. *Phys.Lett.*, B717:396–402, 2012, 1207.0084.

[13] Nikita Blinov, Stefano Profumo, and Tim Stefaniak. The Electroweak Phase Transition in the Inert Doublet Model. *JCAP*, 1507(07):028, 2015, 1504.05949.

[14] Bogumila Swiezewska and Maria Krawczyk. Diphoton rate in the inert doublet model with a 125 GeV Higgs boson. *Phys.Rev.*, D88(3):035019, 2013, 1212.4100.

[15] Michael Gustafsson, Sara Rydbeck, Laura Lopez-Honorez, and Erik Lundstrom. Status of the Inert Doublet Model and the Role of multileptons at the LHC. *Phys. Rev.*, D86:075019, 2012, 1206.6316.

[16] Abdesslam Arhrib, Rachid Benbrik, and Naveen Gaur. $H \to \gamma\gamma$ in Inert Higgs Doublet Model. *Phys.Rev.*, D85:095021, 2012, 1201.2644.

[17] Abdesslam Arhrib, Yue-Lin Sming Tsai, Qiang Yuan, and Tzu-Chiang Yuan. An Updated Analysis of Inert Higgs Doublet Model in light of the Recent Results from LUX, PLANCK, AMS-02 and LHC. *JCAP*, 1406:030, 2014, 1310.0358.

[18] Maria Krawczyk, Dorota Sokolowska, Pawel Swaczyna, and Bogumila Swiezewska. Constraining Inert Dark Matter by $R_{\gamma\gamma}$ and WMAP data. *JHEP*, 1309:055, 2013, 1305.6266.

[19] A. Goudelis, B. Herrmann, and O. Stal. Dark matter in the Inert Doublet Model after the discovery of a Higgs-like boson at the LHC. *JHEP*, 1309:106, 2013, 1303.3010.

[20] Genevieve Belanger, Beranger Dumont, Andreas Goudelis, Bjorn Herrmann, Sabine Kraml, and Dipan Sengupta. Dilepton constraints in the Inert Doublet Model from Run 1 of the LHC. *Phys. Rev.*, D91(11):115011, 2015, 1503.07367.

[21] Nikita Blinov, Jonathan Kozaczuk, David E. Morrissey, and Alejandro de la Puente. Compressing the Inert Doublet Model. *Phys. Rev.*, D93(3):035020, 2016, 1510.08069.

[22] Agnieszka Ilnicka, Maria Krawczyk, and Tania Robens. Inert Doublet Model in light of LHC Run I and astrophysical data. *Phys. Rev.*, D93(5):055026, 2016, 1508.01671.

[23] Agnieszka Ilnicka, Tania Robens, and Tim Stefaniak. Constraining Extended Scalar Sectors at the LHC and beyond. *Mod. Phys. Lett.*, A33(10n11):1830007, 2018, 1803.03594.

[24] Amit Dutta Banik and Debasish Majumdar. Inert doublet dark matter with an additional scalar singlet and 125 GeV Higgs boson. *Eur. Phys. J.*, C74(11):3142, 2014, 1404.5840.

[25] Amit Dutta Banik and Debasish Majumdar. Low Energy Gamma Ray Excess Confronting a Singlet Scalar Extended Inert Doublet Dark Matter Model. *Phys. Lett.*, B743:420–427, 2015, 1408.5795.

[26] Cesar Bonilla, Dorota Sokolowska, Neda Darvishi, J. Lorenzo Diaz-Cruz, and Maria Krawczyk. IDMS: Inert Dark Matter Model with a complex singlet. *J. Phys.*, G43(6):065001, 2016, 1412.8730.

[27] Alexis D. Plascencia. Classical scale invariance in the inert doublet model. *JHEP*, 09:026, 2015, 1507.04996.

[28] Ethan Dolle, Xinyu Miao, Shufang Su, and Brooks Thomas. Dilepton Signals in the Inert Doublet Model. *Phys.Rev.*, D81:035003, 2010, 0909.3094.

[29] Pawel Swaczyna. MSc thesis 2013, University of Warsaw.

[30] Amitava Datta, Nabanita Ganguly, Najimuddin Khan, and Subhendu Rakshit. Exploring collider signatures of the inert Higgs doublet model. *Phys. Rev.*, D95(1):015017, 2017, 1610.00648.

[31] Neng Wan, Niu Li, Bo Zhang, Huan Yang, Min-Fu Zhao, Mao Song, Gang Li, and Jian-You Guo. Searches for Dark Matter via Mono-W Production in Inert Doublet Model at the LHC. *Commun. Theor. Phys.*, 69(5):617, 2018.

[32] A. Belyaev, T. R. Fernandez Perez Tomei, P. G. Mercadante, C. S. Moon, S. Moretti, S. F. Novaes, L. Panizzi, F. Rojas, and M. Thomas. Advancing LHC probes of dark matter from the inert two-Higgs-doublet model with the monojet signal. *Phys. Rev.*, D99(1):015011, 2019, 1809.00933.

[33] P. Poulose, Shibananda Sahoo, and K. Sridhar. Exploring the Inert Doublet Model through the dijet plus missing transverse energy channel at the LHC. *Phys. Lett.*, B765:300–306, 2017, 1604.03045.

[34] Mario Kadastik, Kristjan Kannike, Antonio Racioppi, and Martti Raidal. Implications of the 125 GeV Higgs boson for scalar dark matter and for the CMSSM phenomenology. *JHEP*, 1205:061, 2012, 1112.3647.

[35] Bogumila Swiezewska. Inert scalars and vacuum metastability around the electroweak scale. *JHEP*, 07:118, 2015, 1503.07078.

[36] Najimuddin Khan and Subhendu Rakshit. Constraints on inert dark matter from the metastability of the electroweak vacuum. *Phys. Rev.*, D92:055006, 2015, 1503.03085.

[37] Giovanni Marco Pruna and Tania Robens. Higgs singlet extension parameter space in the light of the LHC discovery. *Phys. Rev.*, D88(11):115012, 2013, 1303.1150.

[38] Tania Robens and Tim Stefaniak. Status of the Higgs Singlet Extension of the Standard Model after LHC Run 1. *Eur.Phys.J.*, C75(3):104, 2015, 1501.02234.

[39] D. de Florian et al. Handbook of LHC Higgs Cross Sections: 4. Deciphering the Nature of the Higgs Sector. 2016, 1610.07922.

[40] M. Espirito Santo, K. Hultqvist, P. Johansson, and A. Lipniacka. Search for neutralino pair production at s**(1/2) from 192-GeV to 208-GeV. 2003.

[41] Albert M Sirunyan et al. Search for invisible decays of a Higgs boson produced through vector boson fusion in proton-proton collisions at $\sqrt{s} = 13$ TeV. *Phys. Lett.*, B793:520–551, 2019, 1809.05937.

[42] Search for dark matter and other new phenomena in events with an energetic jet and large missing transverse momentum using the ATLAS detector. Technical Report ATLAS-CONF-2017-060, CERN, Geneva, Jul 2017.

[43] Manuel Drees, Herbi Dreiner, Daniel Schmeier, Jamie Tattersall, and Jong Soo Kim. CheckMATE: Confronting your Favourite New Physics Model with LHC Data. *Comput.Phys.Commun.*, 187:227–265, 2014, 1312.2591.

[44] Daniel Dercks, Nishita Desai, Jong Soo Kim, Krzysztof Rolbiecki, Jamie Tattersall, and Torsten Weber. CheckMATE 2: From the model to the limit. *Comput. Phys. Commun.*, 221:383–418, 2017, 1611.09856.

[45] Jan Kalinowski, Wojciech Kotlarski, Tania Robens, Dorota Sokolowska, and Aleksander Filip Zarnecki. Benchmarking the Inert Doublet Model for e^+e^- colliders. *JHEP*, 12:081, 2018, 1809.07712.

[46] Leonid Chuzhoy and Edward W. Kolb. Reopening the window on charged dark matter. *JCAP*, 0907:014, 2009, 0809.0436.

[47] Shinya Kanemura, Takahiro Kubota, and Eiichi Takasugi. Lee-Quigg-Thacker bounds for Higgs boson masses in a two doublet model. *Phys.Lett.*, B313:155–160, 1993, hep-ph/9303263.

[48] Andrew G. Akeroyd, Abdesslam Arhrib, and El-Mokhtar Naimi. Note on tree level unitarity in the general two Higgs doublet model. *Phys.Lett.*, B490:119–124, 2000, hep-ph/0006035.

[49] Michael Gustafsson, Erik Lundstrom, Lars Bergstrom, and Joakim Edsjo. Significant Gamma Lines from Inert Higgs Dark Matter. *Phys.Rev.Lett.*, 99:041301, 2007, astro-ph/0703512.

[50] Michel H.G. Tytgat. The Inert Doublet Model: A New archetype of WIMP dark matter? *J.Phys.Conf.Ser.*, 120:042026, 2008, 0712.4206.

[51] Prateek Agrawal, Ethan M. Dolle, and Christopher A. Krenke. Signals of Inert Doublet Dark Matter in Neutrino Telescopes. *Phys.Rev.*, D79:015015, 2009, 0811.1798.

[52] Erik Lundstrom, Michael Gustafsson, and Joakim Edsjo. The Inert Doublet Model and LEP II Limits. *Phys.Rev.*, D79:035013, 2009, 0810.3924.

[53] Chiara Arina, Fu-Sin Ling, and Michel H.G. Tytgat. IDM and iDM or The Inert Doublet Model and Inelastic Dark Matter. *JCAP*, 0910:018, 2009, 0907.0430.

[54] Maria Krawczyk and Dorota Sokolowska. Constraining the Dark 2HDM. In *21st Rencontres de Blois on Windows on the Universe Blois, France, June 21-27, 2009*, 2009, 0911.2457.

[55] Michael Gustafsson. The Inert Doublet Model and Its Phenomenology. *PoS*, CHARGED2010:030, 2010, 1106.1719.

[56] Bogumila Swiezewska. Yukawa independent constraints for two-Higgs-doublet models with a 125 GeV Higgs boson. *Phys.Rev.*, D88(5):055027, 2013, 1209.5725.

[57] Kamakshya Prasad Modak and Debasish Majumdar. Confronting Galactic and Extragalactic γ-rays Observed by Fermi-lat With Annihilating Dark Matter in an Inert Higgs Doublet Model. *Astrophys. J. Suppl.*, 219(2):37, 2015, 1502.05682.

[58] Majid Hashemi, Maria Krawczyk, Saereh Najjari, and Aleksander F. Zarnecki. Production of Inert Scalars at the high energy e^+e^- colliders. 2015, 1512.01175. [JHEP02,187(2016)].

[59] Marco Aurelio Daz, Benjamin Koch, and Sebastin Urrutia-Quiroga. Constraints to Dark Matter from Inert Higgs Doublet Model. *Adv. High Energy Phys.*, 2016:8278375, 2016, 1511.04429.

[60] P. M. Ferreira and Bogumila Swiezewska. One-loop contributions to neutral minima in the inert doublet model. *JHEP*, 04:099, 2016, 1511.02879.

[61] Robinson Longas, Dilia Portillo, Diego Restrepo, and Oscar Zapata. The Inert Zee Model. *JHEP*, 03:162, 2016, 1511.01873.

[62] Majid Hashemi and Saereh Najjari. Observability of Inert Scalars at the LHC. *Eur. Phys. J.*, C77(9):592, 2017, 1611.07827.

[63] Alexandre Alves, Daniel A. Camargo, Alex G. Dias, Robinson Longas, Celso C. Nishi, and Farinaldo S. Queiroz. Collider and Dark Matter Searches in the Inert Doublet Model from Peccei-Quinn Symmetry. *JHEP*, 10:015, 2016, 1606.07086.

[64] Shinya Kanemura, Mariko Kikuchi, and Kodai Sakurai. Testing the dark matter scenario in the inert doublet model by future precision measurements of the Higgs boson couplings. *Phys. Rev.*, D94(11):115011, 2016, 1605.08520.

[65] Debasish Borah and Aritra Gupta. New viable region of an inert Higgs doublet dark matter model with scotogenic extension. *Phys. Rev.*, D96(11):115012, 2017, 1706.05034.

[66] Benedikt Eiteneuer, Andreas Goudelis, and Jan Heisig. The inert doublet model in the light of Fermi-LAT gamma-ray data: a global fit analysis. *Eur. Phys. J.*, C77(9):624, 2017, 1705.01458.

[67] Jan Heisig, Sabine Kraml, and Andre Lessa. Constraining new physics with searches for long-lived particles: Implementation into SModelS. *Phys. Lett.*, B788:87–95, 2019, 1808.05229.

[68] David Eriksson, Johan Rathsman, and Oscar Stal. 2HDMC: Two-Higgs-doublet model calculator. *Comput. Phys. Commun.*, 181:833–834, 2010.

[69] I. F. Ginzburg and K. A. Kanishev. Different vacua in 2HDM. *Phys. Rev.*, D76:095013, 2007, 0704.3664.

[70] Dorota Sokolowska. Temperature evolution of physical parameters in the Inert Doublet Model. 2011, 1104.3326.

[71] Andres Castillo, Rodolfo A. Diaz, John Morales, and Carlos G. Tarazona. Study of vacuum behavior for inert models with discrete Z_2-like and abelian $U(1)$ symmetries. 2015, 1510.00494.

[72] Manfred Lindner, Moritz Platscher, Carlos E. Yaguna, and Alexander Merle. Fermionic WIMPs and vacuum stability in the scotogenic model. *Phys. Rev.*, D94(11):115027, 2016, 1608.00577.

[73] Georges Aad et al. Combined Measurement of the Higgs Boson Mass in pp Collisions at $\sqrt{s} = 7$ and 8 TeV with the ATLAS and CMS Experiments. *Phys.Rev.Lett.*, 114:191803, 2015, 1503.07589.

[74] Measurements of Higgs boson properties from on-shell and off-shell production in the four-lepton final state. Technical Report CMS-PAS-HIG-18-002, CERN, Geneva, 2018.

[75] K.A. Olive et al. Review of Particle Physics. *Chin.Phys.*, C38:090001, 2014.

[76] Guido Altarelli and Riccardo Barbieri. Vacuum polarization effects of new physics on electroweak processes. *Phys. Lett. B*, 253:161, 1991.

[77] Michael E. Peskin and Tatsu Takeuchi. A New constraint on a strongly interacting Higgs sector. *Phys.Rev.Lett.*, 65:964–967, 1990.

[78] Michael E. Peskin and Tatsu Takeuchi. Estimation of oblique electroweak corrections. *Phys.Rev.*, D46:381–409, 1992.

[79] I. Maksymyk, C.P. Burgess, and David London. Beyond S, T and U. *Phys.Rev.*, D50:529–535, 1994, hep-ph/9306267.

[80] Aaron Pierce and Jesse Thaler. Natural Dark Matter from an Unnatural Higgs Boson and New Colored Particles at the TeV Scale. *JHEP*, 0708:026, 2007, hep-ph/0703056.

[81] Philip Bechtle, Oliver Brein, Sven Heinemeyer, Georg Weiglein, and Karina E. Williams. HiggsBounds: Confronting Arbitrary Higgs Sectors with Exclusion Bounds from LEP and the Tevatron. *Comput.Phys.Commun.*, 181:138–167, 2010, 0811.4169.

[82] Philip Bechtle, Oliver Brein, Sven Heinemeyer, Georg Weiglein, and Karina E. Williams. HiggsBounds 2.0.0: Confronting Neutral and Charged Higgs Sector Predictions with Exclusion Bounds from LEP and the Tevatron. *Comput.Phys.Commun.*, 182:2605–2631, 2011, 1102.1898.

[83] Philip Bechtle, Oliver Brein, Sven Heinemeyer, Oscar Stal, Tim Stefaniak, et al. HiggsBounds − 4: Improved Tests of Extended Higgs Sectors against Exclusion Bounds from LEP, the Tevatron and the LHC. *Eur.Phys.J.*, C74(3):2693, 2014, 1311.0055.

[84] Philip Bechtle, Sven Heinemeyer, Oscar Stal, Tim Stefaniak, and Georg Weiglein. Applying Exclusion Likelihoods from LHC Searches to Extended Higgs Sectors. *Eur. Phys. J.*, C75(9):421, 2015, 1507.06706.

[85] http://higgsbounds.hepforge.org.

[86] Vardan Khachatryan et al. Searches for invisible decays of the Higgs boson in pp collisions at sqrt(s) = 7, 8, and 13 TeV. *JHEP*, 02:135, 2017, 1610.09218.

[87] Georges Aad et al. Measurements of the Higgs boson production and decay rates and constraints on its couplings from a combined ATLAS and CMS analysis of the LHC pp collision data at $\sqrt{s} = 7$ and 8 TeV. *JHEP*, 08:045, 2016, 1606.02266.

[88] Philip Bechtle, Sven Heinemeyer, Oscar Stal, Tim Stefaniak, and Georg Weiglein. *HiggsSignals*: Confronting arbitrary Higgs sectors with measurements at the Tevatron and the LHC. *Eur.Phys.J.*, C74(2):2711, 2014, 1305.1933.

[89] N. Aghanim et al. Planck 2018 results. VI. Cosmological parameters. 2018, 1807.06209.

[90] Clifford Cheung, Lawrence J. Hall, David Pinner, and Joshua T. Ruderman. Prospects and Blind Spots for Neutralino Dark Matter. *JHEP*, 05:100, 2013, 1211.4873.

[91] D. Barducci, G. Belanger, J. Bernon, F. Boudjema, J. Da Silva, S. Kraml, U. Laa, and A. Pukhov. Collider limits on new physics within micrOMEGAs_4.3. *Comput. Phys. Commun.*, 222:327–338, 2018, 1606.03834.

[92] E. Aprile et al. Dark Matter Search Results from a One Ton-Year Exposure of XENON1T. *Phys. Rev. Lett.*, 121(11):111302, 2018, 1805.12562.

[93] Alexander Belyaev, James Blandford, and Daniel Locke. Phenodata database. https://hepmdb.soton.ac.uk/phenodata, Jan. 2017.

[94] Qing-Hong Cao, Ernest Ma, Jose Wudka, and C. P. Yuan. Multipartite dark matter. 2007, 0711.3881.

[95] Genevive Blanger, Kristjan Kannike, Alexander Pukhov, and Martti Raidal. Minimal semi-annihilating $\mathbb{Z}_N$ scalar dark matter. *JCAP*, 1406:021, 2014, 1403.4960.

[96] G. Blanger, F. Boudjema, A. Pukhov, and A. Semenov. micrOMEGAs4.1: two dark matter candidates. *Comput. Phys. Commun.*, 192:322–329, 2015, 1407.6129.

[97] Marcin Badziak, Antonio Delgado, Marek Olechowski, Stefan Pokorski, and Kazuki Sakurai. Detecting underabundant neutralinos. *JHEP*, 11:053, 2015, 1506.07177.

[98] Alexander Belyaev, Giacomo Cacciapaglia, Igor P. Ivanov, Felipe Rojas-Abatte, and Marc Thomas. Anatomy of the Inert Two Higgs Doublet Model in the light of the LHC and non-LHC Dark Matter Searches. *Phys. Rev.*, D97(3):035011, 2018, 1612.00511.

[99] Jong Soo Kim, Daniel Schmeier, Jamie Tattersall, and Krzysztof Rolbiecki. A framework to create customised LHC analyses within CheckMATE. *Comput. Phys. Commun.*, 196:535–562, 2015, 1503.01123.

[100] Paolo Nason. A New method for combining NLO QCD with shower Monte Carlo algorithms. *JHEP*, 11:040, 2004, hep-ph/0409146.

[101] Stefano Frixione, Paolo Nason, and Carlo Oleari. Matching NLO QCD computations with Parton Shower simulations: the POWHEG method. *JHEP*, 11:070, 2007, 0709.2092.

[102] Paolo Nason and Carlo Oleari. NLO Higgs boson production via vector-boson fusion matched with shower in POWHEG. *JHEP*, 02:037, 2010, 0911.5299.

[103] Simone Alioli, Paolo Nason, Carlo Oleari, and Emanuele Re. A general framework for implementing NLO calculations in shower Monte Carlo programs: the POWHEG BOX. *JHEP*, 06:043, 2010, 1002.2581.

[104] Torbjorn Sjostrand, Stephen Mrenna, and Peter Z. Skands. PYTHIA 6.4 Physics and Manual. *JHEP*, 05:026, 2006, hep-ph/0603175.

[105] Johan Alwall, Michel Herquet, Fabio Maltoni, Olivier Mattelaer, and Tim Stelzer. MadGraph 5 : Going Beyond. *JHEP*, 1106:128, 2011, 1106.0522.

[106] Torbjoern Sjoestrand, Stefan Ask, Jesper R. Christiansen, Richard Corke, Nishita Desai, Philip Ilten, Stephen Mrenna, Stefan Prestel, Christine O. Rasmussen, and Peter Z. Skands. An Introduction to PYTHIA 8.2. *Comput. Phys. Commun.*, 191:159–177, 2015, 1410.3012.

[107] Bhaskar Dutta, Guillermo Palacio, Jose D. Ruiz-Alvarez, and Diego Restrepo. Vector Boson Fusion in the Inert Doublet Model. *Phys. Rev.*, D97(5):055045, 2018, 1709.09796.

[108] D.S. Akerib et al. First results from the LUX dark matter experiment at the Sanford Underground Research Facility. *Phys.Rev.Lett.*, 112(9):091303, 2014, 1310.8214.

[109] Alejandro Ibarra, Carlos E. Yaguna, and Oscar Zapata. Direct Detection of Fermion Dark Matter in the Radiative Seesaw Model. *Phys. Rev.*, D93(3):035012, 2016, 1601.01163.

[110] M. Aaboud et al. Search for an invisibly decaying Higgs boson or dark matter candidates produced in association with a Z boson in pp collisions at $\sqrt{s} = 13$ TeV with the ATLAS detector. *Phys. Lett.*, B776:318–337, 2018, 1708.09624.

[111] Search for electroweak production of supersymmetric particles in the two and three lepton final state at $\sqrt{s} = 13\,\text{TeV}$ with the ATLAS detector. Technical Report ATLAS-CONF-2017-039, CERN, Geneva, Jun 2017.

[112] M. Aaboud et al. Search for electroweak production of supersymmetric particles in final states with two or three leptons at $\sqrt{s} = 13\,\text{TeV}$ with the ATLAS detector. *Eur. Phys. J.*, C78(12):995, 2018, 1803.02762.

[113] M. Bohm, Ansgar Denner, and H. Joos. Gauge theories of the strong and electroweak interaction. 2001.

[114] Georges Aad et al. Search for supersymmetry at $\sqrt{s} = 13$ TeV in final states with jets and two same-sign leptons or three leptons with the ATLAS detector. *Eur. Phys. J.*, C76(5):259, 2016, 1602.09058.

[115] Morad Aaboud et al. Search for new phenomena in events with a photon and missing transverse momentum in pp collisions at $\sqrt{s} = 13$ TeV with the ATLAS detector. *JHEP*, 06:059, 2016, 1604.01306.

[116] Morad Aaboud et al. Search for new phenomena in final states with an energetic jet and large missing transverse momentum in pp collisions at $\sqrt{s} = 13$TeV using the ATLAS detector. *Phys. Rev.*, D94(3):032005, 2016, 1604.07773.

[117] Morad Aaboud et al. Search for squarks and gluinos in final states with jets and missing transverse momentum at $\sqrt{s} = 13$ TeV with the ATLAS detector. *Eur. Phys. J.*, C76(7):392, 2016, 1605.03814.

[118] Georges Aad et al. Search for gluinos in events with an isolated lepton, jets and missing transverse momentum at $\sqrt{s} = 13$ Te V with the ATLAS detector. *Eur. Phys. J.*, C76(10):565, 2016, 1605.04285.

[119] Georges Aad et al. Search for pair production of gluinos decaying via stop and sbottom in events with b-jets and large missing transverse momentum in pp collisions at $\sqrt{s} = 13$ TeV with the ATLAS detector. *Phys. Rev.*, D94(3):032003, 2016, 1605.09318.

[120] Morad Aaboud et al. Search for top squarks in final states with one isolated lepton, jets, and missing transverse momentum in $\sqrt{s} = 13$ TeV pp collisions with the ATLAS detector. *Phys. Rev.*, D94(5):052009, 2016, 1606.03903.

[121] Morad Aaboud et al. Measurement of the $t\bar{t}Z$ and $t\bar{t}W$ production cross sections in multilepton final states using 3.2 fb^{-1} of pp collisions at $\sqrt{s} = 13$ TeV with the ATLAS detector. *Eur. Phys. J.*, C77(1):40, 2017, 1609.01599.

[122] A search for Supersymmetry in events containing a leptonically decaying Z boson, jets and missing transverse momentum in $\sqrt{s} = 13$ TeV pp collisions with the ATLAS detector. Technical Report ATLAS-CONF-2015-082, CERN, Geneva, Dec 2015.

[123] Search for production of vector-like top quark pairs and of four top quarks in the lepton-plus-jets final state in pp collisions at $\sqrt{s} = 13$ TeV with the ATLAS detector. Technical Report ATLAS-CONF-2016-013, CERN, Geneva, Mar 2016.

[124] Search for top squarks in final states with one isolated lepton, jets, and missing transverse momentum in $\sqrt{s} = 13$ TeV pp collisions with the ATLAS detector. Technical Report ATLAS-CONF-2016-050, CERN, Geneva, Aug 2016.

[125] Search for squarks and gluinos in events with an isolated lepton, jets and missing transverse momentum at $\sqrt{s} = 13$ TeV with the ATLAS detector. Technical Report ATLAS-CONF-2016-054, CERN, Geneva, Aug 2016.

[126] Search for direct top squark pair production and dark matter production in final states with two leptons in $\sqrt{s} = 13$ TeV pp collisions using 13.3 fb^{-1} of ATLAS data. Technical Report ATLAS-CONF-2016-076, CERN, Geneva, Aug 2016.

[127] Further searches for squarks and gluinos in final states with jets and missing transverse momentum at $\sqrt{s} =$13 TeV with the ATLAS detector. Technical Report ATLAS-CONF-2016-078, CERN, Geneva, Aug 2016.

[128] Search for supersymmetry with two and three leptons and missing transverse momentum in the final state at $\sqrt{s} = 13$TeV with the ATLAS detector. Technical Report ATLAS-CONF-2016-096, CERN, Geneva, Sep 2016.

[129] Search for squarks and gluinos in final states with jets and missing transverse momentum using 36 fb^{1} of $\sqrt{s} = 13$ TeV pp collision data with the ATLAS detector. Technical Report ATLAS-CONF-2017-022, CERN, Geneva, Apr 2017.

[130] Search for an invisibly decaying Higgs boson or dark matter candidates produced in association with a Z boson in pp collisions at $\sqrt{s} = 13$ TeV with the ATLAS detector. Technical Report ATLAS-CONF-2017-040, CERN, Geneva, Jul 2017.

[131] Morad Aaboud et al. Search for dark matter and other new phenomena in events with an energetic jet and large missing transverse momentum using the ATLAS detector. *JHEP*, 01:126, 2018, 1711.03301.

[132] Search for new physics in final states with two opposite-sign same-flavor leptons, jets and missing transverse momentum in pp collisions at sqrt(s)=13 TeV. Technical Report CMS-PAS-SUS-15-011, CERN, Geneva, 2015.